Weld World (2016) 60:21–31
DOI 10.1007/s40194-015-0280-x

RESEARCH PAPER

Electron beam welding of aluminum to copper: mechanical properties and their relation to microstructure

C. Otten[1] · U. Reisgen[2] · M. Schmachtenberg[2]

Received: 18 August 2014 / Accepted: 18 November 2015 / Published online: 14 December 2015

Abstract The electrification of the traffic sector increases the importance of the joining of aluminum with copper. During the fusion welding of this joint, brittle intermetallic phases which exert a great influence on the load-bearing capability are developing. Until today, systematic investigations of the different, developing phases neither have been carried out nor has a direct correlation with the mechanical properties been made. Within the scope of this paper, electron beam welding on Al-Cu plates is examined. The focus is put on the identification of the different phases and on their influence on the tensile strength. To this end, the mixture ratio and the energy-per-unit length are varied within the framework of test series. As a result, the microstructure of the welded joint can be characterized via electron backscatter diffraction (EBSD) tests. Further, a direct correlation of these tests with the failure of the welded joint will be made. The greatest weld joint strength of 104 MPa was achieved when the microstructure of the joint featured a lamellar structure, whereas formation of the Al_2Cu phase resulted in brittle fracture of the welded joints along the Al2Cu/lamellar matrix interfaces.

Keywords (IIW Thesaurus) EB welding · Dissimilar materials · Copper · Aluminum

Recommended for publication by Commission IV — Power Beam Processes

✉ C. Otten
ch.otten@focus-gmbh.com

[1] Focus GmbH, Neukirchnerstrasse 2, 65510 Hünstetten-Kesselbach, Germany

[2] Welding and Joining Institute (ISF), RWTH Aachen University, Pontstrasse 49, 52064 Aachen, Germany

1 Introduction

The joining of different materials is, due to the necessity of employing lightweight design concepts, increasingly gaining in importance. Due to the requirement of reducing weight and costs, novel joining methods and material combinations are, therefore, in the focus of industry and research [1]. Particular attention is paid to welded joints made of aluminum and copper. Among other things, this material combination is required for electrically conductive parts [2]. An important, future-orientated application lies in the field of electro mobility and in the production of high-capacity batteries [3]. Aluminum and also copper are characterized by good electrical conductivity; their specific density and the costs for the materials, however, differ significantly. The substitution of copper with aluminum results, on the one hand, in a weight reduction of the manufactured parts and, on the other hand, in cost savings. The positive-substance joining of the dissimilar materials makes special demands to the welding technique since the unwanted formation of intermetallic phases must be specifically controlled and monitored, Fig. 1. In the diagram, the red lines highlighted the different structures which may form during electron beam welding of aluminum to copper.

Tests made about the joining with laser beam [5–7] and with friction welding [8–10] show that it is not possible to completely avoid the formation of intermetallic phases. The detected phases are, at that, varying considerably with regard to number and dimension. Current research work about electron beam welding does not exist although this technology is highly suitable for the joining of dissimilar metal welds [11]. The objective of this work is to determine the characterization of the microstructure of Al-Cu joints on butt joint via electron beam welding and also its influence on the strength.

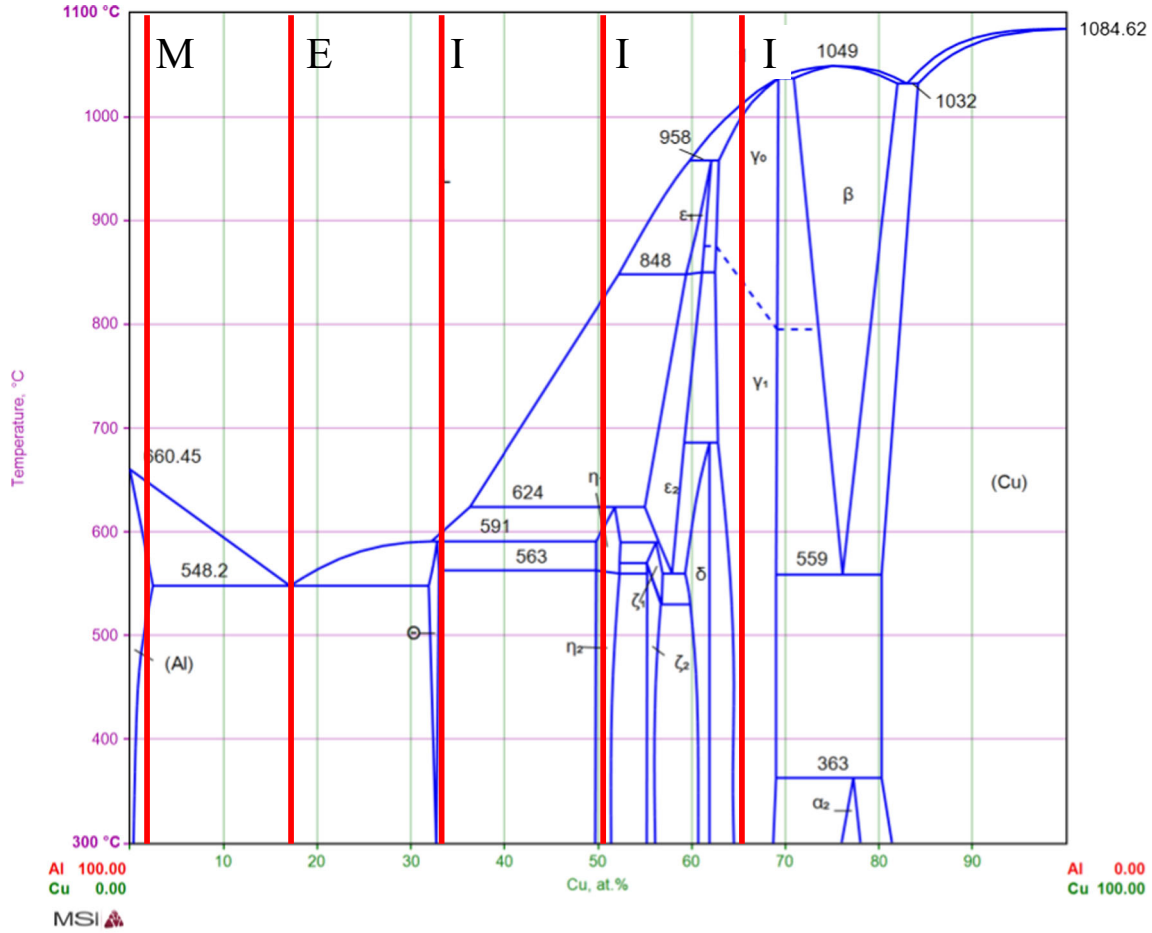

Fig. 1 Phase diagram Al-Cu binary system [4]. The *red lines* clarify the different structures which form during electron beam welding of aluminum to copper. *M* means aluminum-mixed crystal, *E* means eutectic, and *I* represents the different intermetallic phases

2 Materials and methods

In this study, high-purity aluminum and copper sheets of 3-mm thickness were used. The results from the optical emission spectrometry (OES) and the relevant mechanical properties of both materials are listed in Table 1. We are dealing with pure aluminum (99.5 %) and alloyed copper material with a purity of 99.8 %.

In order to exclude a thermally induced change of the material properties, the specimens which had the size of 50 × 55 × 3 mm have been separated mechanically. For the guarantee of the zero gap, the specimens have been milled over their shorter side, Fig. 2. Immediately before the welding process takes place, the specimens have been cleaned chemically with acetone from adhering grease and impurities.

Samples were welded using a FOCUS MEBW micro electron beam welder featuring a maximum acceleration voltage of 60 kV and a beam current of 33 mA which complies with a maximum power of 2 kW. Since the position of the beam determines the composition of the molten metal significantly, the radius and the caustics must be identified. The dimensions and power density distribution of the electron beam were measured using DIABeam diagnostics system [12]. Figure 3 shows a representative measurement of the dimensions and power density of a 60-W e-beam as function of the beam focus current. To obtain better quality

Table 1 OES analysis and mechanical properties of the base material

Alloy	Al	Cu	Si	Fe	σ_{ts} (MPa)	σ_y (MPa)	Hardness (HV)
Al99.5	99.7	<0.001	0.115	0.172	145	85	50
Cu99.8	0.0412	99.8	0.004	0.044	250	110	70

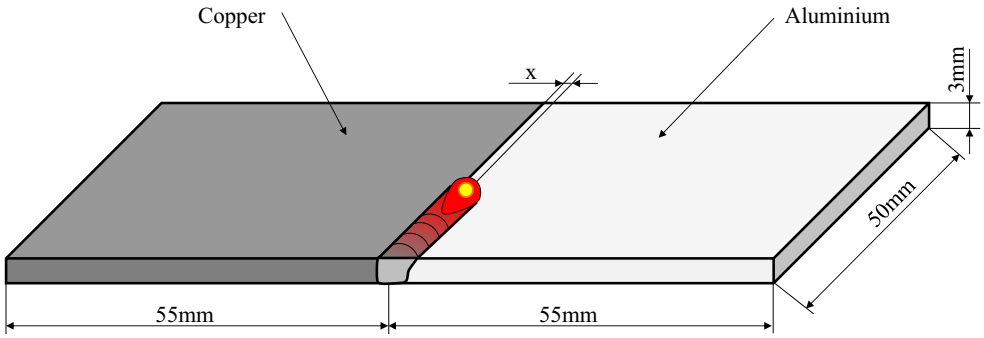

Fig. 2 Schematic representation of EBW process and sheet dimension

weldments, a near-circular (r_{xy}=0.5 mm)-shaped focus electron beam was used.

Electron beam welding of Al-Cu sheets was employed by varying the major process variables such as welding speed, e-beam energy applied per unit length of the weld seam, and beam offset with respect to the Al/Cu interface (shown as "x" in Fig. 2). Defect-free weldments were obtained within a restricted process window, as shown by the blue zone in Fig. 4a. The figure indicates that beam offset values greater than 0.5 mm result in incomplete melting of copper, whereas the offset values smaller than 0.3 mm may lead to formation of intermetallic phases and/or macrocracks. The region where the beam offset is too small is limited by the uncontrolled formation of intermetallic phases, Fig. 11. As from a distance of smaller than 0.3 mm, longitudinal and transversal hardness cracks, due to the formation of intermetallic phases, occur in the weld seam. The offset on the copper side, as in [13, 14], resulted in all cases in the failure of the weld seam during cooling. The asymptotic curve of the energy-per-unit length, plotted in Fig. 4, right, over the welding speed, is explained by the higher process efficiency degree during beam welding with vapor capillary and is in good compliance with [15, 16].

The examinations of the structures were carried out qualitatively by light and electron beam microscopy and quantitatively by energy dispersive X-Ray spectroscopy

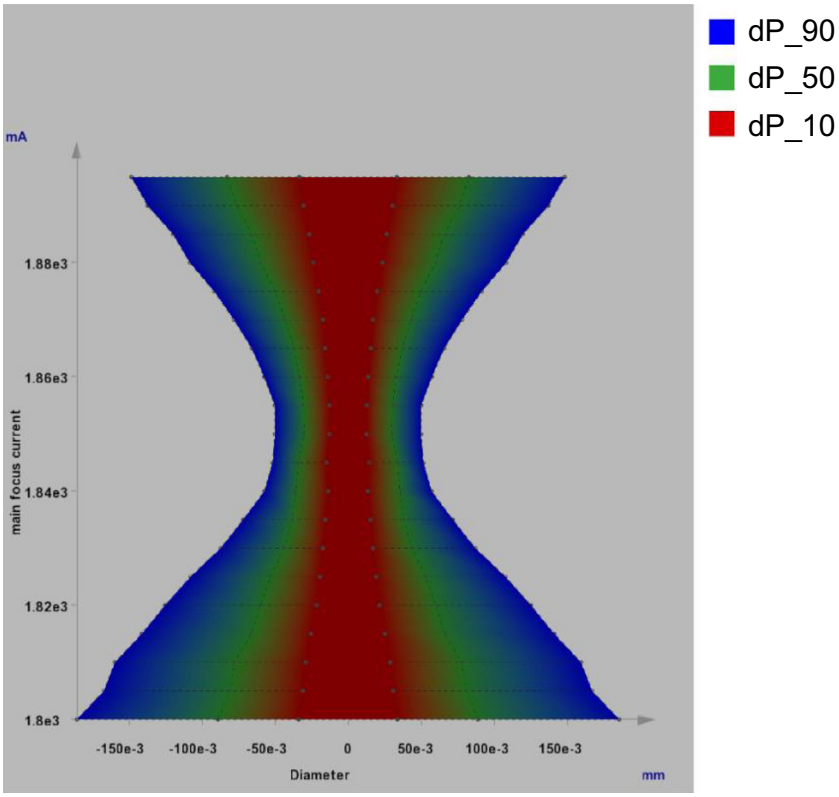

Fig. 3 Beam caustic measurement of the used electron beam machine at 60-kV acceleration voltage and 1-mA beam current

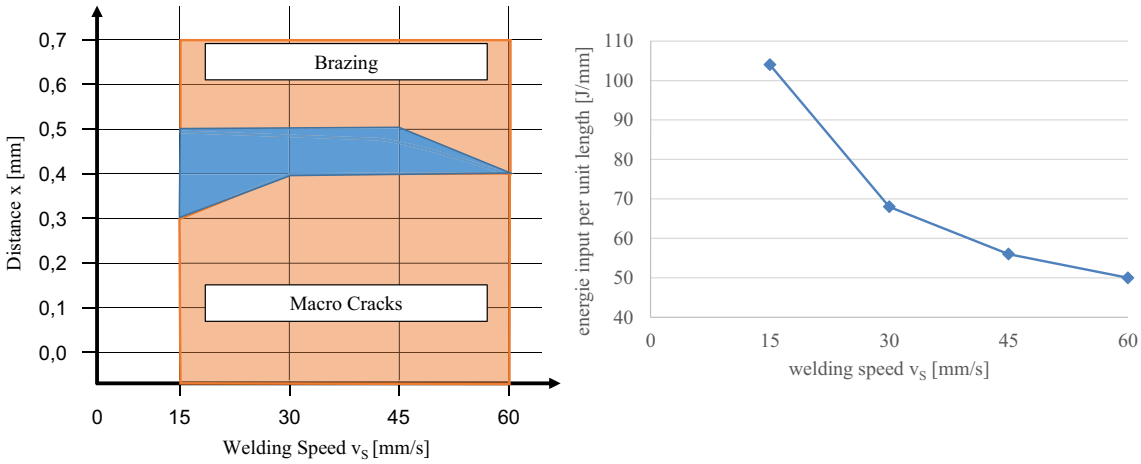

Fig. 4 Process window, the "brazing" area is characterized by an unmelted copper sheet, with lower distance of the beam macrocracks occuring in the weld. In the *right picture*, the energy-per-unit length is shown

(EDS) and different electron backscatter diffraction (EBSD) analyses. The mechanical properties have been determined by hardness measurement in accordance with Vickers and also by tensile tests in accordance with DIN EN ISO 4136 [17]. The tensile tests were carried out by using five specimens in the same section. For the temperature measurements, a thermocouple type K (Ni/CrNi) with a measuring rate of 50 Hz in a distance of 2 mm to the edge of the joint at the top side of the copper sheet is used.

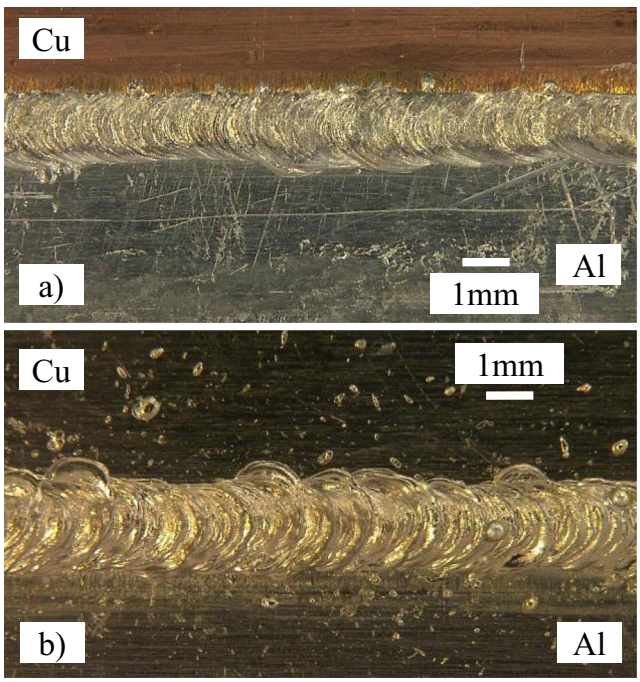

Fig. 5 Weld upper side (**a**) and weld bottom side (**b**) of an electron beam-welded Al-Cu dissimilar material weld

3 Results and discussion

3.1 Microstructure characterization

Figure 5 shows the top and bottom sides of the electron beam-welded Al-Cu joint made by setting a beam offset of 0.4 mm from the Al/Cu interface, towards the aluminum sheet. Complete root penetration and relatively uniform flaking were observed. Macro- and microcracks which normally occur with a smaller beam offset were not detected.

Figure 6a–d shows the backscattered electron image of the weld seam. The three recognizable regions are the two base materials aluminum and copper and also the weld seam which is limited on the aluminum side by the fusion line and on the copper side by a fine phase edge. Weld imperfections such as pores or cracks were not detected. Figure 6b is a magnified image showing Cu/weld seam interface. The weld seam on the left side of the interface features oversaturated aluminum-mixed crystal (M) composed of 3 at.% Cu. This aluminum-rich phase is streaked with copper-rich precipitations. The structure is explained by the fact that due to the decreasing border solubility at decreasing temperature, copper-rich phases are precipitated. Figure 6c shows formation of a layer featuring very fine lamellar structure (region E) adjusted to region M. EDS measurements indicate that region E is composed of 19.9–22.5 at.% Cu; this phase is identified as the eutectic (E) region from aluminum-mixed crystal and Al_2Cu (θ-phase) which is also detected in [18] and [19]. The intermetallic phase I shown in Fig. 6d on the copper side has a fine phase edge. For the determination of the different phases, EBSD and EDS analyses are further carried out.

Figure 6d shows formation of another intermediate layer "I" between region E and pure Cu. EBSD analysis indicates that this intermediate layer has a tetragonal crystal structure

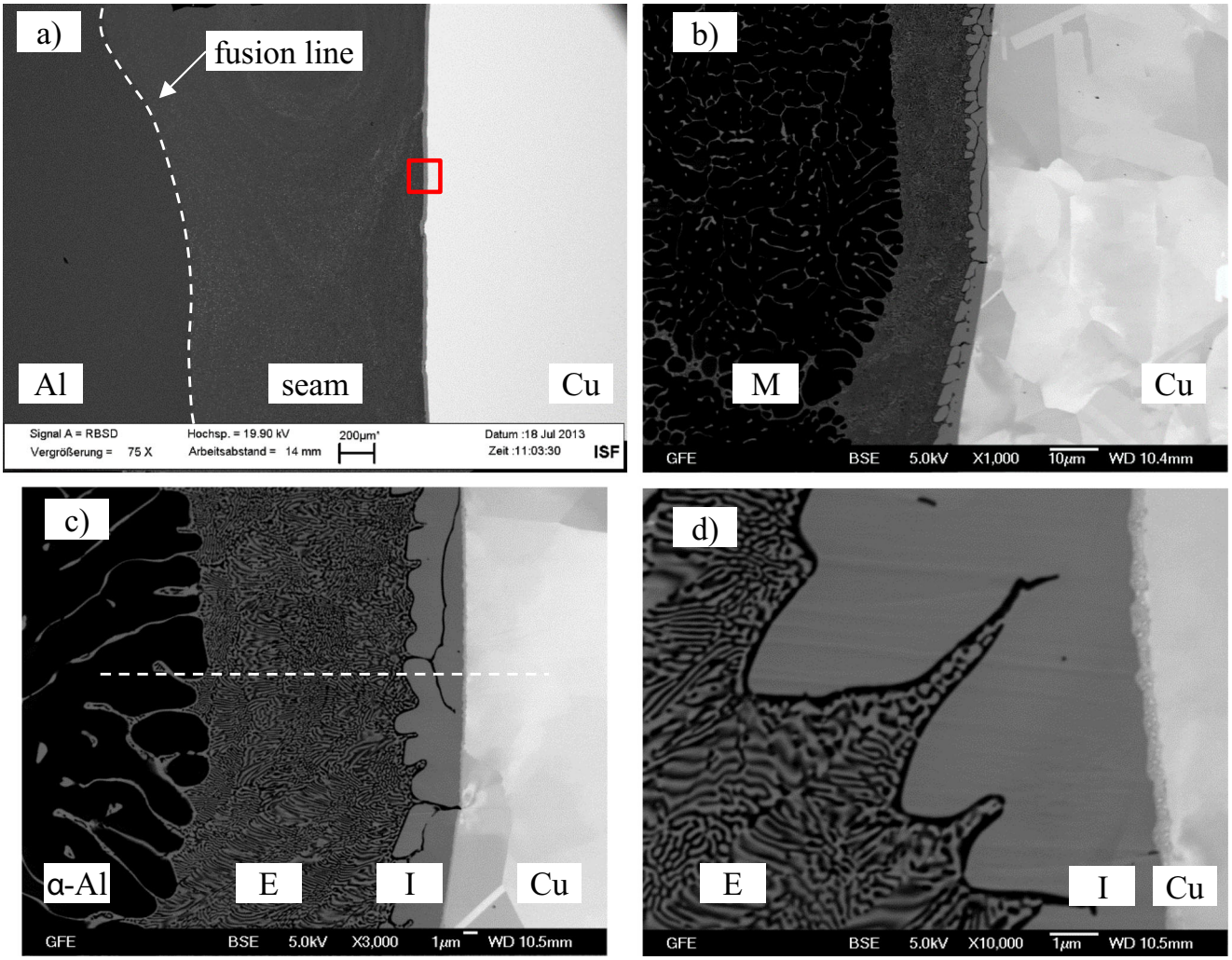

Fig. 6 SEM analysis of an electron beam-welded Al/Cu joint. **a** A characterized overview. **b–d** The interface of the weld with pure copper at different magnifications

(Fig. 7) which corresponds to that of the θ-phase in the Al-Cu phase diagram. The identified phases are illustrated in different colors. The marking is made by means of the lattice structure which has occurred the most frequent in a region. EBSD mapping also identified aluminum-rich regions in yellow, pure copper regions in red, and Al_2Cu-rich regions in green. Due to the homogeneous fcc-lattice structure of aluminum and copper, the differentiation is made by parallel EDS measurements.

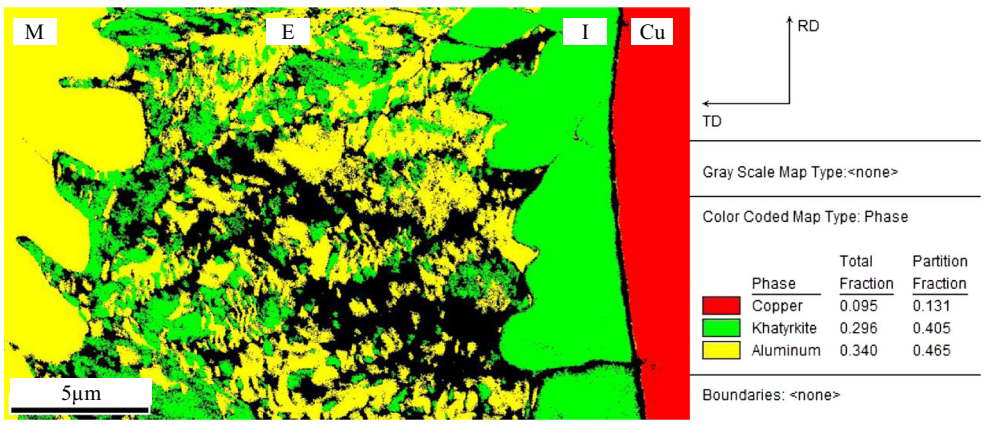

Fig. 7 EBSD color-coded map type. Phase identification. Pure copper dyed in *red*, Al_2Cu in *green*, and pure aluminum in *yellow*

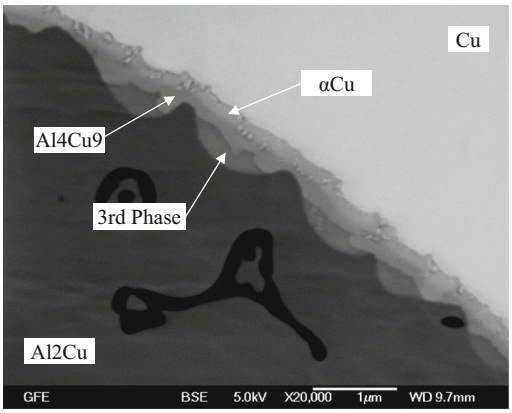

Fig. 8 SEM micrograph at the weld/Cu interface close to the upper surface. Three intermetallic structures can be observed

Cu [at%]	Phase
15	αCu
63-67	Al_4Cu_9
45-60	3rd Phase

If a unique assignment to one of the mentioned phases is not possible, these regions are depicted in black. Regions where different lattice structures occur with the same frequency are also depicted in black. This applies to large areas of the eutectic region. The regions of the eutectic structure (E) where one of the lattice structures occurs more frequently are colored accordingly. It is observed that in the vicinity of the aluminum-mixed crystal, more θ-phase contents exist than in the eutectic structure. Total fraction counts all marks within the different phases. Partition fraction only counts the marks which can be clearly assigned to one structure. Sum-up of the total fraction shows that 26.9 % of the diffraction pattern cannot be assigned by the EBSD software.

A detail of the phase edge between Al_2Cu and Cu made with EDS analysis is shown in Fig. 8. The maximum border solubility of Al in Cu is 19.7 at.% in accordance with [20]. Thus, the measured concentration is 15 at.% aluminum in the region of αCu. Adjacent, a concentration region of 63–67 at.% Al is measured. According to Fig. 1, the Al_4Cu_9 (γ1-phase) lies in this interval. The existence of the γ1-phase as a dominant phase beside Al_2Cu has also been observed by [8, 21] and [22]. It is not possible to unambiguously clarify the third phase via EDS analysis. The high cooling gradient (compare Fig. 10) in electron beam welding may result in a solidification speed which is so high that meta-stable phases can also be established in the solid state. In [8] and [18], it reported about a phase Al_2Cu_3 which has been established via TEM and XRD and which, due to its chemical composition, comes into question as the third phase. According to [21, 23] and [24], Al-Cu is developing as the third phase after Al_2Cu and Al_4Cu_9. Gueydan et al. [25] show the boundary layer structure: α-Al-Al_2Cu-AlCu-Al_4Cu_9-α-Cu after thermal aging of copper-coated aluminum wires. While the eutectic structure and the θ-phase are highly uniform over the entire boundary layer, the phase edge is strongly varying between Al_2Cu and Cu. The γ1- and the third phase can be detected via REM only in the upper part of the weld seam. The largest part of the boundary layer between Al_2Cu and Cu looks similar as in Fig. 6d and consists thus mainly of a copper-mixed crystal.

The crystallographic orientation of the individual grains within the regions shown in Fig. 7 can be visualized in color by the inverse pole figure (IPF) orientation map, Fig. 9. The map allows to draw conclusions about the solidification

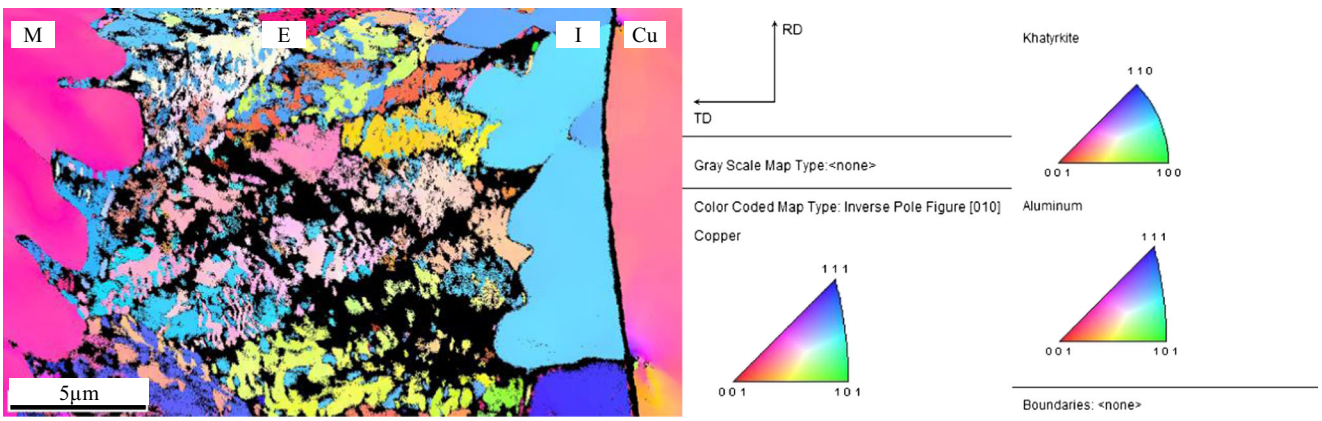

Fig. 9 EBSD color-coded map type. Inverse pole figure (010) shows the growth direction during the solidification

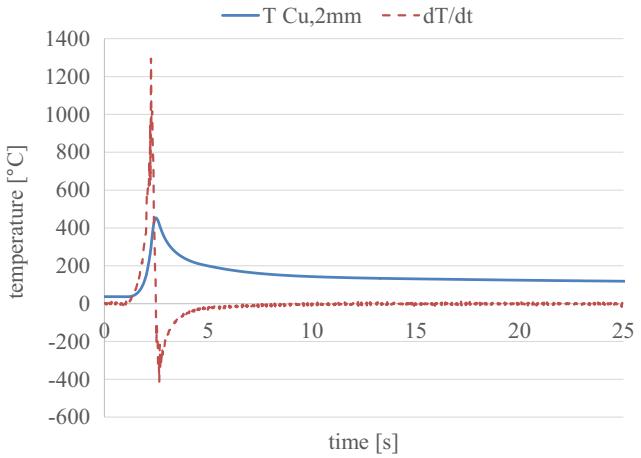

Fig. 10 Temperature gradient, measured on the copper sheet with a distance of 2 mm to the edge of the joint

direction and, thus, about the phase growth. Weld seam solidification occurs from the outside to the inside.

Due to the divergent heat conductivity values (Al99.5 at RT 224.7 (W/mK) [26] and Cu at RT 390 (W/mK)), the solidification is shifted in the direction of the copper. The θ-phase (I) and αAl show a directed growth into the eutectic phase. This must, as a consequence, have solidified as the last region of the weld seam at a temperature of 548 °C. It is not possible to unambiguously specify the growth of the γ1- and of the third phase in this paper. Since these phases are also detected in tests about friction stir welding where the process temperatures are clearly below the melting temperatures of both metals [27, 28], a phase growth during the cooling phase by solid-phase diffusion is also possible. [9] and [24] specify that proceeding from the assumption of a volume diffusion, the phase growth of the Al_2Cu phase follows a parabolic growth law.

The temperature gradient which is depicted in Fig. 10 was measured using a thermocouple type K at a distance of 2 mm from the edge of the joint on the copper sheet. Due to the peak temperatures during electron beam welding of aluminum of approximately 1900 °C [29], the tactile measurement of the molten metal itself is not possible. In the diagram, moreover, the first dissipation of the temperature is plotted over the time (dT/dt). Curves which are typical of beam welding with high heating (>1290 °C/s) and cooling gradients (>400 °C/s) can be observed. The time-temperature integral has a significant influence on the formation of intermetallic phases [30, 31]. The specimens which have been examined in this work have intermetallic phase width values of 3–6 µm. An influence of the welding speed which may affect the energy-per-unit length and the cooling gradient has not been observed. The reason may be the small difference of the temperature-time integral of more/higher than 300 °C. The intermetallic phases start forming, at temperatures of 120 to 400 °C [23]. However, within this temperature range, the growth rates of these intermetallic phases were reported to be very slow [9].

The influence of the beam offset, however, has significant influence on the seam formation and on the width of the intermetallic phases, Fig. 11. Based on the backscattered image contrast, it can be deduced that as the beam offset decreases, the Cu content of the weld seams becomes greater (brighter gray tones). Al concentrations in the α-mixed crystal are constant at approximately 3 %. The eutectic structure in the weld seam is, however, increasing considerably. In the specimen with the distance of 0.3 mm, agglomeration of the θ-phase occurs. The phase γ1 and the third phase develop, at that, exclusively in the boundary layer to the copper.

3.2 Mechanical properties and fracture behavior

The investigation about the influence of the beam offset on the mechanical properties is carried out via hardness measurement and quasi-static tensile tests. Figure 12a shows the hardness measurements taken across the joints electron beam welded by using different beam offset values of 0.4 and 0.3 mm. The measurements have been carried out centrically across the weld seam. The hardness profile across the weld seam made by using 0.4-mm offset exhibited a linear-like increase indicating an increase in Cu concentration and increased fraction

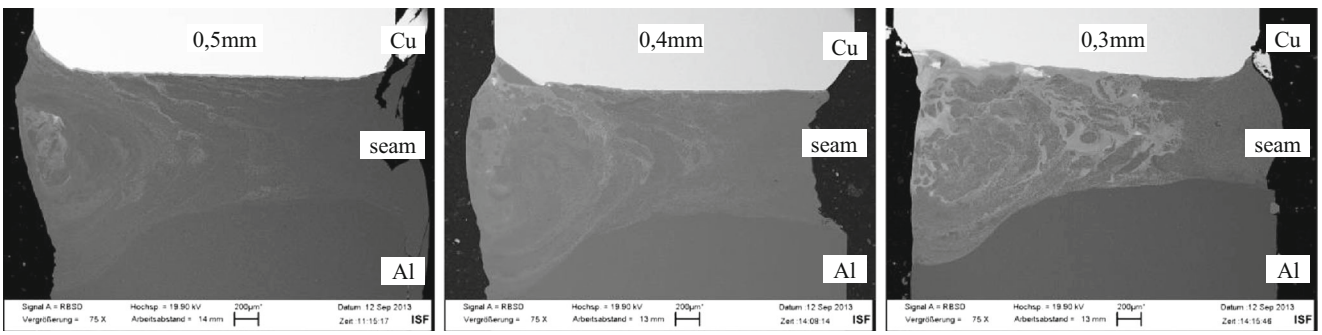

Fig. 11 SEM micrographs of electron beam-welded Al-Cu seams with different distances towards the edge of the joint

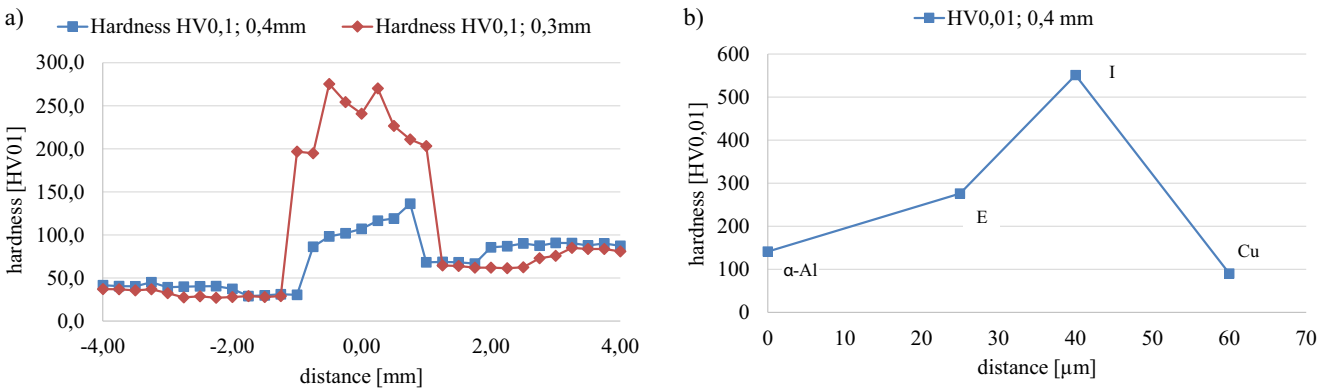

Fig. 12 Hardness measurements HV0.1 across the complete weld (**a**) and HV0.01 of the interface weld/pure copper (**b**)

of eutectic structure (α-Al+θ-phase) towards the weld seam/Cu interface. On the other hand, the hardness profile of the weld seam made by using 0.3-mm beam offset can be attributed to even dispersion of the eutectic structure (region E) throughout the weld seam. Figure 12b depicts a hardness measurement with HV0.01 along the dashed line in Fig. 6c. The hardness of the eutectic structure (E) was 276 HV which is consistent with the measurements reported in [28] and [32]. The hardness of the θ-phase region was 551 HV. Minor deviations from the measurements reported in [30] and [33] may be explained by the tongue-shaped morphology of the phase and, caused by that, the lack of the supportive effect.

The evaluation of the tensile tests is depicted in Fig. 13. The stress-strain diagram shows exemplary two graphs, a welded aluminum specimen and an Al-Cu joint. It is shown that the formation of Al-Cu-mixed crystal leads to higher tensile strength. The maximum tensile strength of 104 MPa has been achieved with a beam offset of 0.4 mm. Almost all tensile specimens failed in brittle fracture tests with an elongation after fracture of maximally 3 %. In the tests with 0.4 mm, some of these specimens show areas of ductile failure. The minor scattering within the individual specimens is explained by the high beam quality and the exact positioning of the beam with the used equipment technique. Larger distances to the edge of joints resulted in the decrease of strength values. As from 0.5-mm distance, the face of the copper sheet is no longer completely molten and a joint is developing which is composed, on the aluminum side of a welded seam and, on the copper side, of a brazed joint. Since these joints did not fit to the requirements of a weld, no further analysis was performed. The influence of the microstructure in the weld seam on the tensile strength is discussed by means of the fracture surfaces.

The copper-side fracture surface of a specimen with a distance of 0.4 mm is shown in Fig. 14a, and it can basically be divided into three different regions. Those are clearly differing by their different copper concentrations. The region A1 is increased in Fig. 14b and is characterized by fine lamellar eutectic structure (E) with included mixed crystals. The fracture path in this region leads through a region where both phases exist. In the considered specimen, the distance to the copper is approximately 25 µm. The identification of the phase regions A2 and A3 is carried out in addition to the morphology via EDS-point measurements, Table 2. In Fig. 14c, the middle region is identified as eutectic due to its morphology and copper content of 23 at.% The medium-gray region shows the typical topography of a brittle fracture. The measured copper content is on the copper and also on the aluminum side at 62–63 at.%. This means that the fracture path at this point is going through the intermetallic phase Al_2Cu as has also been observed by [21]. The region A3, as shown in Fig. 14c, exhibited the highest Cu concentration and thus can be identified as Al_4Cu_9. A fine-grained structure is

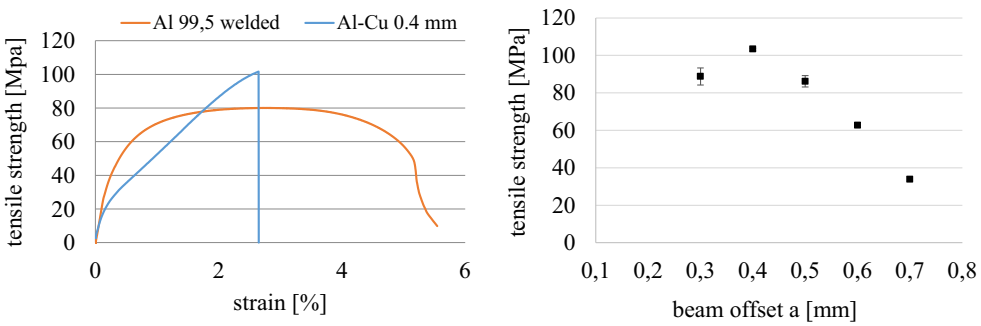

Fig. 13 Stress-strain curve and values of electron beam-welded Al-Cu joints with a welding speed of 15 mm/s over the distance to the weld seam

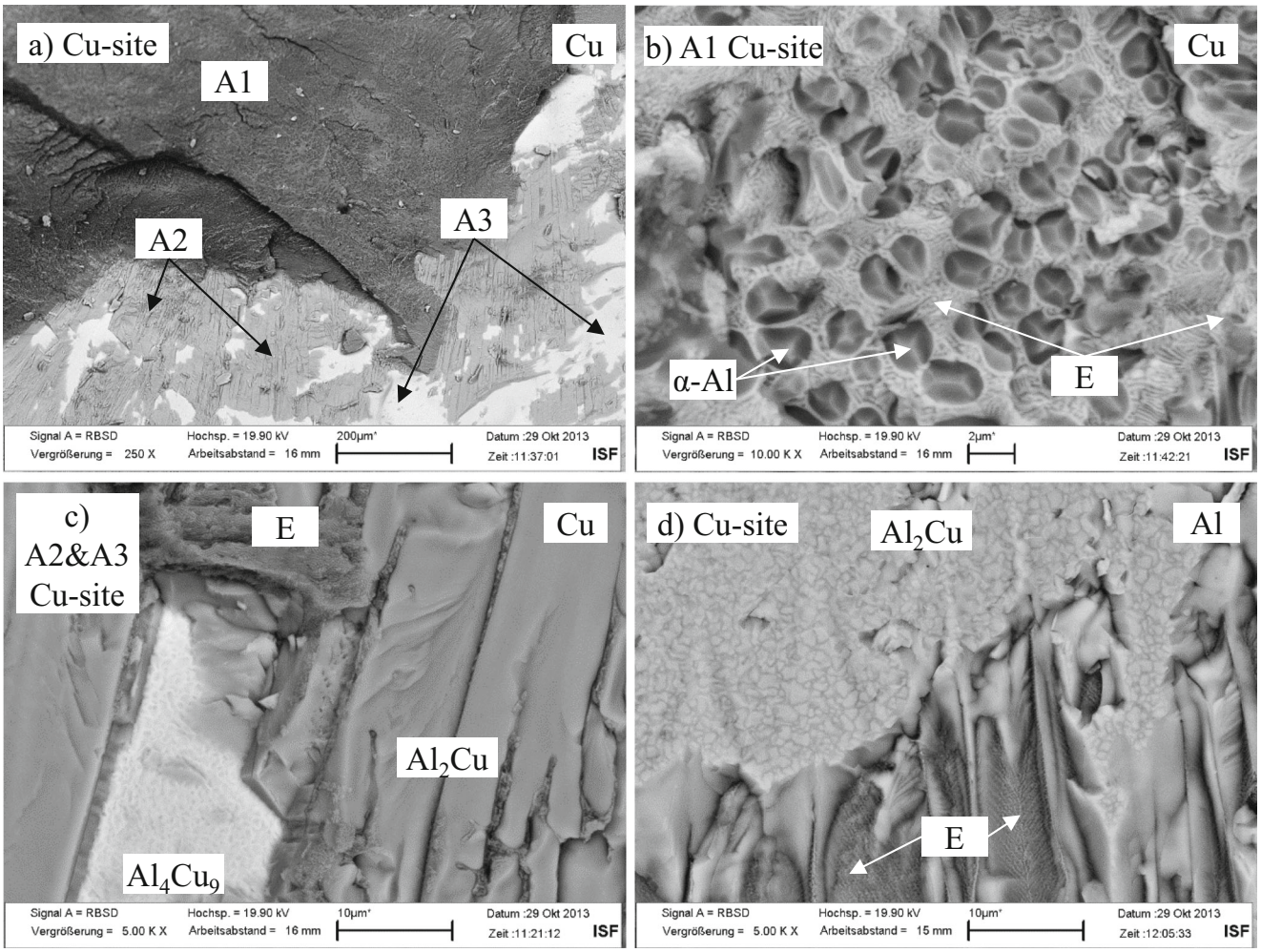

Fig. 14 Fracture surfaces of a specimen with a distance of 0.4 mm. **a** Overview (Cu). **b** Magnification region A1 (Cu). **c** Magnification region A2 and A3 (Cu). **d** region Al

observed which exists also on the aluminum side, Fig. 14d. The EDS measurements show, however, that at this point, we are dealing with Al_2Cu. The crack path may thus be in the boundary layer between the γ1- and the θ-phases. According to [23], a phase width Al_4Cu_9 smaller than 100 nm

Table 2 EDX measurement of the fracture surfaces

Area	Site	Al (at.%)	Cu (at.%)	Phase
A1	Cu	76.587	23.412	Eutectic
A1	Cu	76.404	23.596	Eutectic
A2	Cu	61.810	38.190	Al_2Cu
A2	Cu	61.819	38.181	Al_2Cu
A3	Cu	33.835	66.165	Al_4Cu_9
A3	Cu	31.793	68.207	Al_4Cu_9
A2	Al	63.140	36.860	Al_2Cu
A2	Al	63.112	36.888	Al_2Cu

allows to produce good metallurgical joints between Al and Cu. The phase width values which were detected in this phase are similar.

The weld seams 0.4 and 0.5 mm consist mainly of the aluminum-mixed crystal which was dispersed with eutectic precipitations. The exception is the approx. 5 % of the copper-side weld seam which consists of the specified structure (E)+(I), Fig. 6c. The proportion of the eutectic precipitations is in the specimens with a distance of 0.4 mm higher than in those with a distance of 0.5 mm. A possible explanation for the higher strength values is the ductility of the eutectic structure which can reduce internal stresses by plastic deformation. Highly deformed and recrystallized regions in the microstructure show typically high values of the local misorientation [34]. These misorientations can be represented with EBSD KAM maps (Kernel Average Misorientation) by the comparison of crystal orientation of two neighboring measuring points, Fig. 15. Green/red represents regions with residual stresses while the blue regions

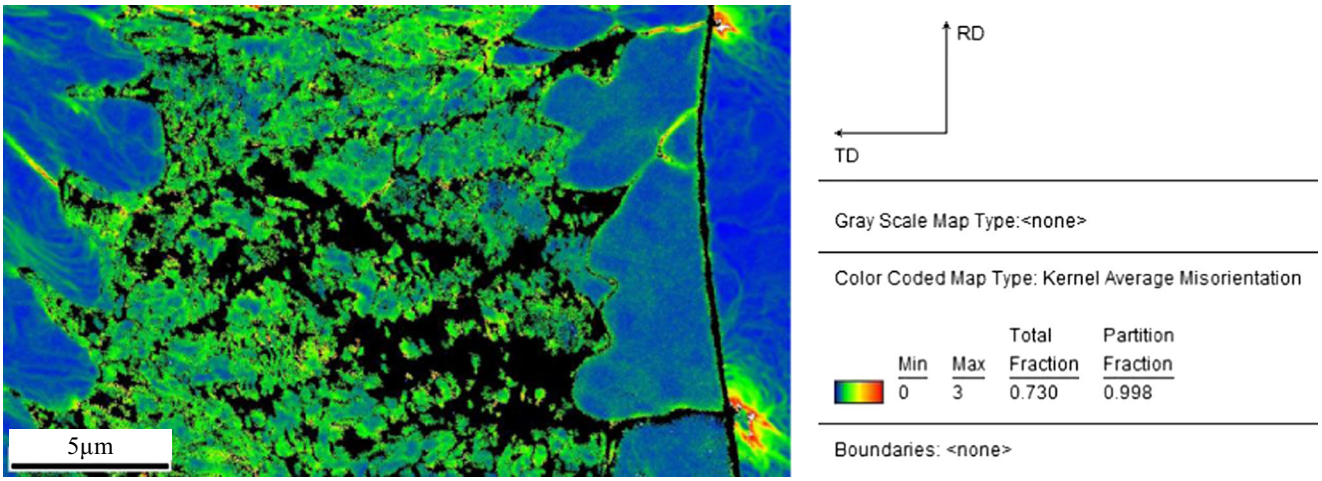

Fig. 15 EBSD color-coded map type. Kernel Average Misorientation shows the internal stresses

have low stresses. The eutectic structure shows increased but, however, homogeneous stress distribution. The low stress within the intermetallic phase Al_2Cu is remarkable. The highest stresses are in the region of the copper where the grain boundaries of the intermetallic meet one another.

The fracture of this specimen may thus have occurred under tensile load, as in Fig. 16. Crack initiation has occurred at highly deformed grain boundaries within the intermetallic phase (1). The propagation is, in the beginning, along the boundary line between the γ1- and the θ-phases and subsequently through the θ-phase (2) into the eutectic phase region [12] (3). This means that the binding between Al_2Cu and Al_4Cu_9 is worse than that between Al_4Cu_9 and the Cu-mixed crystal.

4 Conclusion

Sound welds of the material combination aluminum-copper were produced by micro electron beam welding. It has been shown that the controlling of the melting ratio of metals is an important factor for defect-free welding of these dissimilar metals. The ratio can be controlled by the beam position. A deflection of 0.4 mm on the aluminum sheet achieves a tensile strength of 104 MPa which is higher compared to a similar aluminum weld.

Due to locally restricted energy of the high-power electron beam, the heat input can be controlled which directs to short interaction times. Thus, an uncontrolled formation of brittle intermetallic can be avoided.

The study of the fracture surface permits the presentation of a possible fracture mechanism of Al-Cu dissimilar joints. After that, the crack starts in highly deformed regions inside the intermetallic layer.

Besides demonstration of the influence of the microstructure to the mechanical properties, the results of the present study can be used for further investigations, like the corrosion, crash, and electronic behavior of this combination.

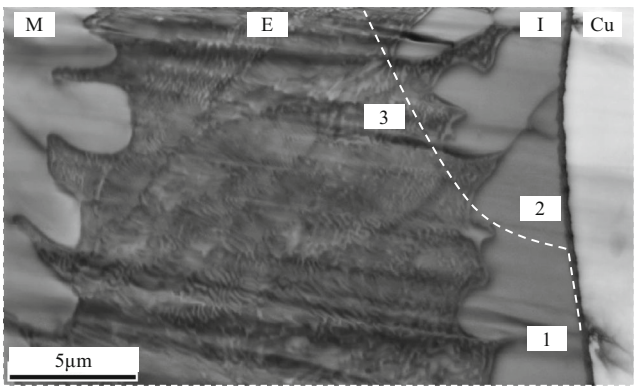

Fig. 16 Possible fracture mechanism of an electron beam-welded Al-Cu dissimilar joint

References

1. Dilthey U, Stein L (2006) Multimaterial car body design: challenge for welding and joining. Sci Technol Weld Join 11(2):135–142
2. Zhao Y, Li D, Zhang Y (2013) Effect of welding energy on interface zone of Al-Cu ultrasonic welded joint. Sci Technol Weld Join 18(4): 354–360
3. Hailat M, Mian A, Chaudhury Z, Newaz G, Patwa R, Herfurth H (2012) Laser micro-welding of aluminum and copper with and without tin foil alloy. Microsyst Technol 18:103–112
4. Gröbner J (2004) Al-Cu binary phase diagram evaluation. MSI, Materials Science International Services GmbH, Stuttgart
5. Mai TA, Spowage AC (2004) Characterisation of dissimilar joints in laser welding of steel-kovar, copper-steel and copper-aluminum. Mater Sci Eng A 374:224–233
6. Lee SJ, Nakumura H, Kawahito Y, Katayama S (2014) Effect of welding speed on microstructural and mechanical properties of

laser lap weld joints in dissimilar Al and Cu sheets. Sci Technol Weld Join 19(2):111–118
7. M Weigl, A Grimm, M Schmidt (2011) Laser-welded connections for high-power electronics in mobile systems. Electr Drives Prod Conf (EDPC) 88–92
8. Tan C, Jiang ZG, Li L, Chen Y, Chen X (2013) Microstructural evolution and mechanical properties of dissimilar Al-Cu joints produced by friction stir welding. Mater Des 51:466–473
9. Lee W-B, Bang KS, Jung S-B (2005) Effects of intermetallic compound on the electrical and mechanical properties of friction welded Cu/al bimetallic joints during annealing. J Alloys Compd 390:212–219
10. Firouzdor V, Kou S (2012) Al-to-Cu friction stir lap welding. Metall Mater Trans A 43:303–315
11. Sun Z, Karppi R (1996) The application of electron beam welding for the joining of dissimilar metals: an overview. J Mater Process Technol 59(3):257–267
12. A Backhaus, S Ufer, J. de Vries (2013) Präzise Vermessung des Elektronenstrahls mit einem neuartigen Sensor - Technologietransfer gelungen! in Im Blickpunkt - Deutschlands Elite Institute: Institut für Schweißtechnik und Fügetechnik der RWTH Aachen University, Aachen, Institut für Wissenschaftliche Veröffentlichungen und der ALPHA Imformationsgesellschaft mbH, 40–42
13. Zürn H, Dorn L (1966) Untersuchungen über das Schweißen unterschiedlicher Metalle mit dem Elektronenstrahl. DVS-Berichte 1:69–87
14. Bandov H (1971) Beitrag zum Verbinden von Aluminum mit Kupfer durch Elektronenstrahlschweißen. Schweißen und Schneiden 23(7):274–277
15. Sánchez-Amaya JM, Boukha Z, Amaya-Vázquez MR, Botana FJ (2012) Weldability of aluminum alloys with high-power diode laser. Weld J 91:155–161
16. Lee CH, Kim SW, Yoon EP (2000) Electron beam welding characteristics of high strength aluminum alloys for express train applications. Sci Technol Weld Join 5(5):277–283
17. N. N., DIN EN ISO 4136 (2013) Zerstörende Prüfung von Schweißverbindungen an metallischen Werkstoffen. Deutsches Institut für Normung e.V, Berlin
18. Xia C, Li Y, Puchkov UA, Gerasimov SA, Wang J (2008) Microstructure and phase constitution near the interface of Cu-Al vacuum brazing using Al-Si filler metal. Vacuum 82:799–804
19. Aravind M, Yu P, Yau MY, Ng DH (2004) Formation of Al2Cu and AlCu intermetallics in Al(Cu) alloy matrix composites bey reaction sintering. Mater Sci Eng A 380:384–393
20. Massalaski TB (1990) Binary alloy phase diagrams, 2nd edn. ASM International, Ohio
21. Chen C-Y, Chen H-L, Hwang W-S (2006) Influence of interfacial structure development on the fracture mechanism and bond strength of aluminum-copper bimetal plate. Mater Trans 47(4):1232–1239
22. Genevois C, Girard M, Huneau B, Sauvage X, Racineux G (2011) Interfacial reaction during friction stir welding of Al and Cu. Metall Mater Trans A 42A:2290–2295
23. Lee KS, Lee SE, Sung HK, Lee DH, Kim JS, Chang YW, Lee S, Kwon YN (2013) Influence of reduction ratio on the interface microstructure and mechanical properties of roll-bonded Al/Cu sheets. Mater Sci Eng A 583:177–181
24. Abassi M, Taheri AK, Salehi MT (2000) Growth rate of intermetallic compounds in Al/Cu bimetal produced by cold roll welding process. Alloy Compounds 319:233–241
25. Gueydan A, Domengés B, Hug E (2014) Study of intermetallic growth in copper-clad aluminum wires after thermal aging. Intermetallics 50:34–42
26. Spittel M, Spittel T (2011) "Al99,5", in The Landolt-Börnstein Database. Springer-Verlag, Berlin Heidelberg, pp 1–7
27. Lui HJ, Shen JJ, Zhou L, Thao YQ, Lui C, Kuang LY (2011) Microstructural characterisation and mechanical properties of friction stir welded joints of aluminum alloy to copper. Sci Technol Weld Join 16(1):92–98
28. Ouyang J, Yarrapareddy E, Kovacevic R (2006) Microstructural evolution in the friction stir welded 6061 aluminum alloy (T6-temper condition) to copper. Mater Proc Technol 172(1):110–122
29. DA Schauer, WH Gied, SM Shintaku (1987) Electron beam welding cavity temperature distributions in pure metals and alloys. Weld J 127–133
30. Chen C-Y, Hwang W-S (2007) Effect of annealing on the interfacial structure of aluminum-copper joints. Mater Trans 48(7):1938–1947
31. C Otten, U Reisgen, J Schönberger (2014) Investigations about the influence of the time-temperature curve on the formation of intermetallic phases during electron beam welding of steel-aluminum material combination, Weld World
32. Zhang Y, Yamane T, Hirao K, Minamino Y (1991) Microstructures and Vickers hardness of rapidly solidified Al-Cu alloys near the Al-Al2Cu equilibrium eutectic composition. J Mater Sci 26:5799–5805
33. Sarvghad-Moghaddam M, Parvizi R, Davoodi A, Haddad-Sabzevar M, Imani A (2014) Establishing a correlation between interfacial microstructures and corrosion initiation sites in Al/Cu joints by SEM-EDS and AFM-SKPFM. Corrsion Sci 79:148–158
34. Konrad J, Zaefferer S, Raabe D (2006) Investigation of orientation gradients around a hard Laves particle in a warm-rolled Fe3Al-based alloy using 3D EBSD-FIB technique. Acta Mater 54:1369–1380